

Spectroscopic analysis of different types of single-wall carbon nanotubes

H. KUZMANY¹, B. BURGER¹, M. HULMAN¹, J. KÜRTI²
A. G. RINZLER³ and R. E. SMALLEY³

¹ *Universität Wien, Institut für Materialphysik - Strudlhofgasse 4, A-1090 Wien, Austria*

² *Eötvös University, Department for Biological Physics
Puskín U. 5-7, H-1088 Budapest, Hungary*

³ *Department of Chemistry, Rice University - Houston, TX 77005, USA*

(received 25 May 1998; accepted in final form 1 October 1998)

PACS. 78.30-j – Infrared and Raman spectra.

PACS. 78.66Qn – Polymers; organic compounds.

PACS. 63.20Dj – Phonon states and bands, normal modes, and phonon dispersion.

Abstract. – The Raman response of the radial breathing mode in single-wall carbon nanotubes was analyzed for excitation with 10 different laser lines. The line shape was fitted with 14 Voigtian oscillators which could be correlated to tubes of different helicity. The strongest lines were observed between 172 and 199 cm^{-1} . For an assignment frequencies evaluated from a density functional calculation and scattering intensities for the resonance transitions were used. The 5 strongest lines observed are consistent with scattering from tubes with 11 different helicities. From the evaluation of the scattering intensities the nearest-neighbor integral between two carbon atoms on the curved sheet was found to be 2.6 ± 0.5 eV.

Since the discovery of carbon nanotubes this material attracts increasing interest in the community of scientists studying nanomaterials. However, the fundamental properties of the individual tubes could not be investigated until a technology was provided to prepare large amounts of single-wall nanotubes (SWNTs). This possibility was first demonstrated by Thess *et al.* [1] using laser evaporation of a graphite target doped with 2% Ni/Co catalyst. The resulting tubes were found to have a rather uniform diameter and to condense into bundles or ropes with a triangular structure. From the X-ray analysis the length of the unit cell for this structure is 1.7 nm, corresponding to a diameter of 1.38 nm for the individual tubes.

At this point the quantitative descriptions of the structure and electronic properties of cylindrical graphene sheets became important as they were developed a few years before [2,3]. The single-wall tubes consist of a graphene sheet rolled up along an arbitrary lattice vector with components (n, m) . Tubes with $n = m$ are labeled *armchair*, tubes with either $n = 0$ or $m = 0$ are labeled *zigzag*. All other tubes are *chiral*. The observed diameter of 1.38 nm is consistent with (10, 10) and (17, 0) tubes.

The rolled-up graphene sheet represents an exactly one-dimensional lattice with the fun-

damental lattice vector \mathbf{T} along the tube axis. Armchair nanotubes are metallic. The other types of tubes are quasi-metallic if $n - m$ is a multiple of 3.

The band structure and the density of states for the tubes can be obtained by the zone folding technique. This yields subbands with sharp peaks in the density of states for the π and for the π^* band. Since these peaks are approximately symmetric to the Fermi level, the joint density of states resonates between symmetric pairs and optical transitions will resonate as a consequence. For small enough tubes the resonance energy depends on the tube diameter. Using the force constants for a flat graphene sheet, approximate frequencies were obtained [4,5] and revealed for some of the mode frequencies a dependence on the diameter of the tube, if the latter is smaller than about 2 nm.

A situation where vibrational frequencies and electronic transition energies depend on the size of particles is appropriate for photoselective resonance scattering in Raman experiments as it is very well known for conjugated polymers. In this case the exciting laser selects a fraction of particles for which resonance conditions are fulfilled. The result is a shift of the Raman lines with the energy of the exciting laser. This effect was recently observed for single-wall nanotubes by Rao *et al.* [5]. Another recent result reported diameter-dependent Raman scattering for the high-frequency E_{2g} derived mode located around 1600 cm^{-1} [6].

From the calculations in [4] the radial breathing mode (RBM) of the tubes was expected to give the best information on the type and diameter of the tubes. Thus, we performed a detailed Raman analysis of this mode. Preliminary results of this study were reported before [7,8] and exhibited the contribution of a rather large number of tubes to this line in full agreement with a recent analysis of similar tube material by scanning tunneling microscopy [9]. The work presented here provides a more refined analysis in a sense that a wider spectral range for the excitation of the spectra was used, the Raman cross-sections were evaluated explicitly, a reliable and high-level evaluation of the mode frequencies was used, and more credit is given to contributions from chiral tubes. The Raman response in all recorded spectra was found to have a fine structure consisting of a rather large but well-defined number of discrete lines. Using the first-principle calculations for the mode frequencies these lines could be assigned to a distribution of armchair, zigzag, and chiral tubes. The result is important for future work on growth and cleaning conditions of SWNTs. For the strongest lines the spectroscopic properties and in turn information on the electronic structure of the cylindrical graphene sheets could be obtained. The evaluation was consistent with a nearest-neighbor overlap integral of $2.6 \pm 0.5 \text{ eV}$ in agreement with recent results from tunneling spectroscopy on single tubes [9] (2.7 eV) and a value derived from LDA calculations [10] (2.5 eV).

SWNTs were prepared by the two-beam laser desorption process and deposited on a cold finger [1]. The as-grown material was excited in front of a Raman spectrometer at ambient conditions with lasers in the near infrared (NdYAG at 1.16 eV) and in the visible spectral range. For the line shape analysis 9 different laser lines in the spectral range from 1.6 eV to 2.7 eV were used. The laser power was about 1 mW focused with a cylindrical lens. The spectra were recorded with 2 cm^{-1} resolution. They were completely stable with irradiation time and highly independent of the position on the sample. No difference between as-grown and purified tubes was recorded for the frequency range of the RBM.

The overall Raman spectrum as excited with 1.16 eV or in the visible spectral range showed two strong lines at 179 cm^{-1} and just below 1600 cm^{-1} . The low-frequency and the high-frequency lines originate from the RBM and from the tangential carbon stretching, respectively. In the following we concentrate on the response from the RBM. The three plots of fig. 1 show a selection of spectra excited with three representative laser lines. The shape, structure and peak position of the lines depend strongly on the energy of the exciting laser.

To represent the whole set of the 9 spectra oscillators were first selected by inspection. A

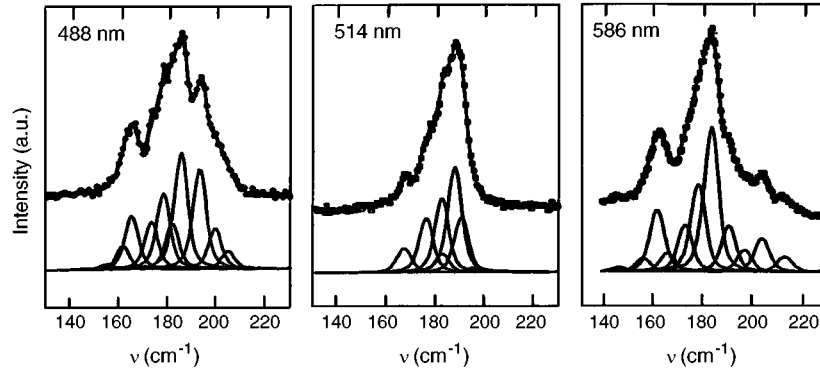


Fig. 1. – Raman response for the radial breathing mode of single-wall carbon nanotubes as excited with three different lasers. The full drawn lines are Voigtians resulting from a fitting procedure. Their sum yields the full drawn line through the experimental points.

fitting to the experimental results with Voigtian response curves reproduced the spectra with a set of lines of more or less constant frequencies —for all 9 spectra the result from the fits revealed only $\pm 2 \text{ cm}^{-1}$ variation for the oscillators— and a small distribution of widths. With the assumption that all components of the spectra originate from the same set of tubes the 9 spectra were then fitted again with a final set of 14 oscillators where the widths were kept constant at $7 \pm 1 \text{ cm}^{-1}$. As a result a set of 14 oscillators was obtained, each dressed with intensities related to the exciting lasers. The frequencies for the set are listed in table I, line one. They extend from 147 cm^{-1} to 230 cm^{-1} .

Scattering intensities for the spectra excited with the different laser lines were determined by calibrating the spectrometer using published results for the resonance of the F_{1g} mode in Si [11]. The strongest lines were observed, with decreasing intensity, for 185, 177, 195, 172, and 199, respectively. The first three lines were clearly stronger than the rest.

Table I lists also vibrational frequencies evaluated from a density functional calculation with a local density approximation [12]. The package used for this calculation was proved to be appropriate to evaluate carbon systems [13] and revealed excellent results for the evaluation of the radial breathing mode of C_{60} . With the standard parameter set for carbons the frequency for this mode was evaluated close to the experimental error which is about 1%. Line two and

TABLE I. – *Vibrational oscillators used to fit the experimentally observed Raman lines of the radial breathing mode of single-wall carbon nanotubes (line 1). Also listed are frequencies calculated by a density functional method [12] for armchair tubes (line 2) and zigzag tubes (line 4). The values in parentheses (lines 3 and 5) are n from (n, n) and $(n, 0)$, respectively.*

observed lines	147	156	162	167	172	177	182	185	190	195	199	206	211	230
calculated for armchair tubes	146		159			175				195			219	
	(12)		(11)			(10)				(9)			(8)	
calculated for zigzag tubes		158		167		177		187			200		214	231
		(19)		(18)		(17)		(16)			(15)		(14)	(13)
chiral tubes	172	.	182	.	190	.	.	206	.	.

line four in the table were evaluated for armchair tubes and for zigzag tubes, respectively. The excellent agreement of the frequency for the (10, 10) tube (175 cm^{-1}) with the observed mode at 177 cm^{-1} makes it almost certain that the (10, 10) armchair tubes contribute to this line. *Ab initio* evaluation of the frequencies for the chiral tubes was not possible since the unit cell is too large. However, using the results for the armchair and zigzag tubes the frequencies for the chiral tubes can savely be evaluated from their diameter D using the $1/D$ scaling law.

With the above assignment for the (10, 10) tubes an excellent agreement between experiments and calculation was obtained for the rest of the modes. Two different sets are easily identified. The first set with frequencies 147, 162, 177, and 195 cm^{-1} is consistent with armchair tubes with (n, n) decreasing from (12, 12) to (9, 9). The second set with frequencies 156, 167, 177, 185, 199, 211, and 230 cm^{-1} is consistent with zigzag tubes with $(n, 0)$ decreasing from (19, 0) to (13, 0). Note that the modes for two tubes ((10, 10) and (17, 0)) overlap completely so that they cannot be distinguished from each other if only the frequency is considered.

The line at 172 and a few other small lines located at 182, 190, and 206 cm^{-1} could not be identified in this way. It is very suggestive to assign them to chiral tubes. There is indeed a large number of possibilities for chiral tubes in the expected diameter range, about 15 species between (10, 10) and (9, 9), for example. This means there may be other overlaps with the armchair and zigzag tubes as is indicated by the dots in line 6 of the table. Thus, in contrast to the highly selective results from electron diffraction on nanotube ropes [14] the presence of a considerable number of armchair tubes, zigzag tubes and chiral tubes is demonstrated to exist in the material.

The scattering intensities (Raman cross-sections) are an other experimental signature which can be used to identify the tubes and to study their electronic structure. To make use of this, the Raman cross-section has to be evaluated. Since the cross-section is strongly related to the density of states, it is expected to exhibit very sharp resonances as a consequence of the van Hove singularities in the latter. The density of states $g(\epsilon)$ can be evaluated from the band structure $\epsilon(k, q, n, m, \gamma)$ by $g(\epsilon) = |\partial\epsilon/\partial k|^{-1}$. The band structure for a tube with arbitrary vector (m, n) is given by

$$\begin{aligned} \epsilon(k, q, n, m, \gamma) = \pm\gamma \left\{ 1 + 2 \left[\cos \left(\frac{\sqrt{3}ka}{2} \frac{m}{(n^2 + m^2 + nm)^{1/2}} + q\pi \frac{2n + m}{n^2 + m^2 + nm} \right) + \right. \right. \\ \left. \left. + \cos \left(-\frac{\sqrt{3}ka}{2} \frac{n}{(n^2 + m^2 + nm)^{1/2}} + q\pi \frac{n + 2m}{n^2 + m^2 + nm} \right) \right] + \right. \\ \left. + 2 \left[1 + \cos \left(\frac{\sqrt{3}ka}{2} \frac{m + n}{(n^2 + m^2 + nm)^{1/2}} + q\pi \frac{n - m}{n^2 + m^2 + nm} \right) \right] \right\}^{1/2}. \quad (1) \end{aligned}$$

a and γ are the lattice constant of the graphene sheet and the next-neighbor overlap integral, respectively. q is the subband index extending from 0 to $N/2$ where $N = 2(n^2 + m^2 + nm)/d_R$ is the number of subbands in the conduction band and in the valence band, respectively. d_R is the largest common divisor between $2n + m$ and $2m + n$. For each subband k extends from $-\pi/T$ to π/T , where T is the length of the unit cell. From a comparison between LDA calculations and tight-binding calculations γ was found to be 2.5 eV for the rolled-up graphene sheet [10].

For a symmetry between valence band and conduction band the joint density of states $g_{j\text{d}}$ is identical to the density of states except for a factor two in the energy, and thus immediately

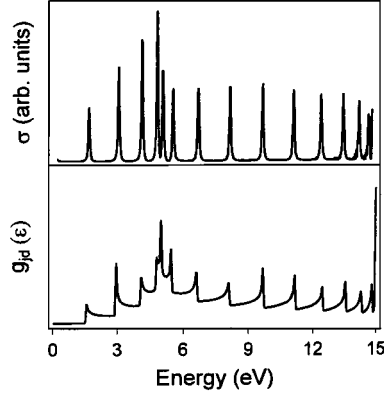


Fig. 2. – Joint density of states $g(\epsilon)$ and Raman cross-section σ for the (10, 10) tubes.

evaluated from (1). The Raman cross-section σ is obtained from [15]

$$\sigma(\omega_i) \propto \left| \int \frac{M_f M_{ph} M_0 g_{jd}(\epsilon) d\epsilon}{(\hbar\omega_i - \epsilon - i\hbar\Gamma)(\hbar\omega_s - \epsilon - i\hbar\Gamma)} \right|^2. \quad (2)$$

ω_i and ω_s are the frequencies of the incident and scattered light, respectively, and $1/\Gamma$ is the lifetime of the excited state. The product of the matrix elements in the numerator represents the initial excitation of the electron, the generation of the phonon, and the de-excitation from the excited state. For the evaluation of σ the product of the matrix elements was assumed to be independent of the energy. An example for the joint density of states and the cross-section is shown in fig. 2 for the (10, 10) tubes and $\gamma = 2.6$ eV. The sharp resonances in both functions are evident.

Interestingly the chiral tubes were found to exhibit similar resonances as the armchair and zigzag tubes even though there can be a very large number of branches in the band structure. For the chiral tube (13, 5), *e.g.*, 518 subbands are distributed across only 7.5 eV. Even though 516 of them are twofold degenerated, 260 different branches remain. In spite of this the density of states exhibits only 19 resonances. This is very similar to the number of resonances for a (16, 0) tube. This result is in agreement with a recent discussion of the density of states for chiral tubes [16, 17].

For the five strongest lines reliable results for the relative scattering intensities could be evaluated. In all cases low scattering intensities were recorded in the central part of the spectral range used for excitation and a more or less strong increase of the scattering was observed at the red and blue end of the excitation. An example is shown in fig. 3a, b for the modes at 177 and 185 cm^{-1} . The response is characteristically different in the high-energy and in the low-energy range. Whereas the cross-sections increase dramatically on both edges of the spectrum for the line at 177 cm^{-1} , it remains rather flat on the high-energy side for the line at 185 cm^{-1} and has already passed the resonance on the low-energy side. There is a weak intermediate resonance around 2.4 eV in both cases. The maximum recorded enhancement of the cross-section for the 177 cm^{-1} line is a factor 10 in the deep blue and a factor 25 in the deep red. For the 185 cm^{-1} line it is only 1.7 in the blue but 28 in the red.

The assignment of the oscillator at 177 cm^{-1} to the (10, 10) tubes is consistent with the calculation but not unique. In fact, considering all chiralities five tubes are possible within an uncertainty of $\pm 2 \text{ cm}^{-1}$. However, from a consistency between the evaluated and observed

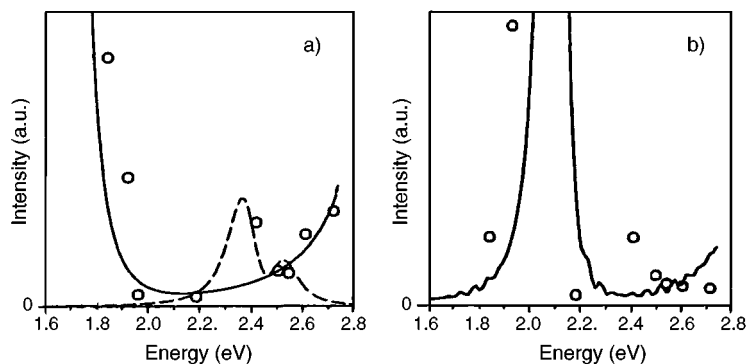


Fig. 3. – Comparison between observed relative scattering intensities (\circ) and calculated Raman cross-section ($—$) for two modes at 177 (a) and 185 cm^{-1} (b), respectively. The dashed line in (a) is for a (17, 0) tube.

resonant transition energies only (10, 10) and (14, 5) remain as candidates. The full drawn line in fig. 3a is the cross-section calculated for (10, 10) tubes and $\gamma = 2.6$ eV.

The intermediate resonance around 2.4 eV may originate from the (17, 0) tubes which exhibit the same frequency as the (10, 10) or (14, 5) tubes. The dashed line reflects the resonance cross-section evaluated from the inverse derivative of (1) together with (2) for the same value of γ but with a smaller scaling factor for the absolute intensity. This scaling factor can be considered as describing the concentration of the scatterer.

For the resonance of the line at 185 cm^{-1} shown in fig. 3 we can proceed similarly but the experimental values in the red are now on the decreasing edge of the resonance. From the evaluation of the frequencies several candidates exist but considering the transition energies only two remain, namely (16, 0) and (14, 4). The full drawn line in the figure is calculated for (16, 0) with $\gamma = 2.55$ eV. The intermediate maximum around 2.4 eV must originate from a chiral tube with the same frequency. In table II we have listed characteristic data for several chiral tubes which exhibit a RBM frequency located ± 2 cm^{-1} from 185 cm^{-1} . Since the resonance width is expected to be less than ± 1 cm^{-1} as seen from fig. 3, the only candidate is the (13, 5) tube.

The three other strong lines were found to be consistent with (17, 1) and (13, 7) (for 172 cm^{-1}), (13, 4) and (9, 9) (for 195 cm^{-1}), and (14, 2) and (15, 0) (for 199 cm^{-1}).

Summarizing we have analyzed the fine structure of the Raman response of the RBM in

TABLE II. – Frequencies and optical transitions energies ϵ_i for chiral tubes with frequencies around 185 cm^{-1} .

tube (n, m)	chiral angle (degree)	RBM (cm^{-1})	ϵ_1 (eV)	ϵ_2 (eV)	ϵ_3 (eV)
(10, 9)	28.3	183	2.12	3.04	3.36
(15, 2)	6.2	187	2.07	2.99	3.31
(13, 5)	15.6	187	2.31	2.55	3.72
(14, 4)	12.2	184	2.05	2.87	3.30
(11, 8)	24.8	185	1.63	1.7	3.12

single-wall carbon nanotubes and found a rather large number of tubes with different helicities as the source for this structure. Helicities extended from armchair to tubes with various chiralities including zigzag species. Using first-principle calculations for the RBM an absolute correlation between the observed modes and the corresponding tube was established at least for armchair and zigzag structures. Chiral tubes were found to exhibit similar resonances as the nonchiral species. For the strongest observed species a spectroscopic analysis could be provided for the optical transitions.

Work supported by the FFWF in Austria, project P-11943-phy and the HSF OTKA T022980 in Hungary. Nanotube research at Rice University was supported by the NSF, the Texas Advanced Technology Program, and the R. A. Welch Foundation. We acknowledge valuable discussions with G. KRESSE (T.U. Wien), and A. KASUYA (Tohoku U.).

REFERENCES

- [1] A. THESS *et al.*, *Science*, **273** (1996) 483.
- [2] JISHI R. A. *et al.*, *J. Phys. Soc. Jpn.*, **63** (1994) 2252.
- [3] HAMADA N. *et al.*, *Phys. Rev. Lett.*, **68** (1992) 1579.
- [4] JISHI R. A. *et al.*, *Chem. Phys. Lett.*, **209** (1993) 77.
- [5] RAO A. *et al.*, *Science*, **275** (1997) 187.
- [6] KASUYA A. *et al.*, *Phys. Rev. Lett.*, **78** (1997) 4434.
- [7] KUZMANY H. *et al.*, *Physica B*, **244** (1998) 186.
- [8] KUZMANY H. *et al.*, *Carbon*, **36** (1998) 709.
- [9] WILDÖER J. W. *et al.*, *Nature*, **391** (1998) 59.
- [10] MINTMIRE J. W. and WHITE C. T., *Carbon*, **33** (1995) 893.
- [11] RENUCCI J. B., TYTE R. N. and CARDONA M., *Phys. Rev. B*, **11** (1975) 3885.
- [12] KÜRTI J. *et al.*, *Phys. Rev. B*, **58** (1998) 8869.
- [13] KRESSE G. and HAFNER J., *Phys. Rev. B*, **49** (1994) 14251.
- [14] COWLEY J. M. *et al.*, *Chem. Phys. Lett.*, **97** (1997) 379.
- [15] MARTIN R. M. and FALICOV L. M., *Topics Appl. Phys.*, **8** (1983) 79.
- [16] WHITE C. T. and MINTMIRE J. W., *Nature*, **394** (1998) 29.
- [17] CHARLIER J. C. and LAMBIN P., *Phys. Rev. B*, **57** (1998) 15037.